Modeling and control of an Antagonistic Shape Memory Alloy Actuator

André Ianagui, andre.ianagui@gmail.com
Eduardo Aoun Tannuri, eduat@usp.br
Escola Politécnica da Universidade de São Paulo – Departamento de Mecatrônica e Sistemas Mecânicos
Av. Prof. Luciano Gualberto, travessa 3, nº 380 - CEP 05508-010 - São Paulo – SP, Brazil

Abstract. *This work presents the modeling, grey-box parameter estimation and control design of a force-cooled antagonistic shape memory alloy (SMA) rotational actuator. The model is based on a sub-layer phase transformation approach, taking account the large non-linearities that rise from the phase-transformation dynamics (in special, the highly hysteretic dynamics). A Quadratic Sequential Algorithm is used to estimate the model parameters and fit the real data of a tested bench model in the modeled parameters. At last, two model-referenced control schemes, both nonlinear, are designed and simulated using the estimated model, each in force and position control modes. The first control scheme is a nonlinear feedback linearization, which does not take account eventual model or parameter error effect. Then, a nonlinear sliding mode controller with limit layer, more robust to eventual mismatch in modeling and state estimation is introduced and simulated. Both are then compared in terms of stability, dynamic response and cut-off frequency.*

Keywords*: Shape Memory Alloy, Nonlinear Control, Sliding Mode Control, Modeling*

1. INTRODUCTION

Shape Memory Alloys are metallic materials that have the interesting characteristic of retrieving its original form or size after subjected to heating. This characteristic, known as "memory effect", has been shown to be very useful in several applications, from prosthesis to mechanical couplings, electrical connections and actuators (Otubo et al., 1997).

The memory effect is explained by changes in the crystalline structure of the material. At low temperatures, the alloy is in its martensitic form, presenting a tetragonal (BCT) crystal structure. In this phase, the yield point is very low, making its mechanical behavior under load plastic and allowing easy deformation. When heated, the alloy changes its phase to austenite, with a face centered cubic (FCC) crystal structure. This phase has the characteristic of having a very high yield stress, causing the material to contract. In the usual application as actuator, the material is deformed at the cold phase due to applied load, and then heated to cause its contraction and consequent movement.

The crystal structure changes that occur in the thermal process described above are thermodynamically irreversible, resulting in temperature hysteresis. Even though the heating process can be quick (it is usually based on joule effect), most of its dynamic performance is limited by the cooling process, which is based on (relatively low speed) heat conduction/convection. To enhance the cooling dynamic response, Romano and Tannuri (2007) proposed a system using Seebeck-Peltier effect tablets, enhancing this system's dynamic response in their posterior work (2009) by configuring the actuator in an antagonistic setup. This configuration also makes output symmetric with respect to negative or positive control input.

The control system used in these actuators must be able to absorb the nonlinearities due to the phase transformation process, in special the hysteresis. Even though PID controllers are robust and usually have good dynamics, better performance can be achieved by using nonlinear controllers. Romano and Tannuri (2009) compared the two control methods, concluding that a Sliding Mode Controller (SMA) was a better choice due to its large capacity of absorbing modeling and parameter errors. Cut off frequency of 1.14 Hz was obtained, against 0.89 Hz of PID controllers. Both were applied to control angular position of the output axis. In an attempt to enhance the dynamic response even further, this work introduces modeling and parameter estimation of the antagonistic actuator proposed then.

Most authors present position control schemes, but an important application would be force tracking control systems. In a robotic grip, for instance, having a correct amount of force applied to the object that is being hold is essential not to damage the object with too much force or to drop it. As light and silent actuators, SMA's are very well suited to this task, eliminating the mechanical issues from the usual pneumatic or hydraulic open loop systems.

Grant and Hayward (2000) have shown that force tracking control was achievable, but used simple modeling and control, facing issues with the appearance of limit cycles. Its bandwidth was up to 2.00 Hz. Choi et al. (2001) also presented good control of applied force in a robotic grip, using a $\mathcal{H}_\infty$ controller, but achieving a bandwidth of 0.48 Hz. Teh and Featherstone (2007) obtained similar results to Grant's, but using simple PID controllers and ignoring the nonlinearities of the system. Finally, Elahinia et al. (2004) used sliding mode controllers and a PID associated with feedback linearization method. Even though most of the force tracking works use antagonistic setups, all of them used natural cooling methods, which may have reduced the bandwidth.

The main advantages of the SMA actuators are their high power/density ratio, maintainability, reliability and clean silent operation. Between its disadvantages are the low energy efficiency due to conversion of heat to mechanical energy, inaccurate motion control due to hysteresis, nonlinearities, parameter uncertainties, difficulty in measuring variables such as temperature, and slow response due to the thermal process involved in the working principle.

2. EXPERIMENTAL SETUP

The controlled object consists in a rotating axis actuated by two SMA wires assembled in an antagonistic setup. In the front end of the axis a bean is connected to a light mass, to simulate the moment of inertia of the load, in a standard pendulum configuration. The bean can be substituted by a flexure measuring load cell, in order to measure the force/torque applied in the lower end of the bean. A precision potentiometer is attached to the back end of the shaft, in order to measure angular position. Two peltier effect tablets are positioned in contact with the wires, to enhance cooling capacity. Figure 1 illustrates the mechanical setup. The axis diameter is 9 mm, the bean length is 45 mm and the mass is of approximately 45 grams. The SMA wires are made of Nitinol, having 150 mm length and an approximate diameter of 0.2 mm, according to the supplier, Dynalloy, Inc.

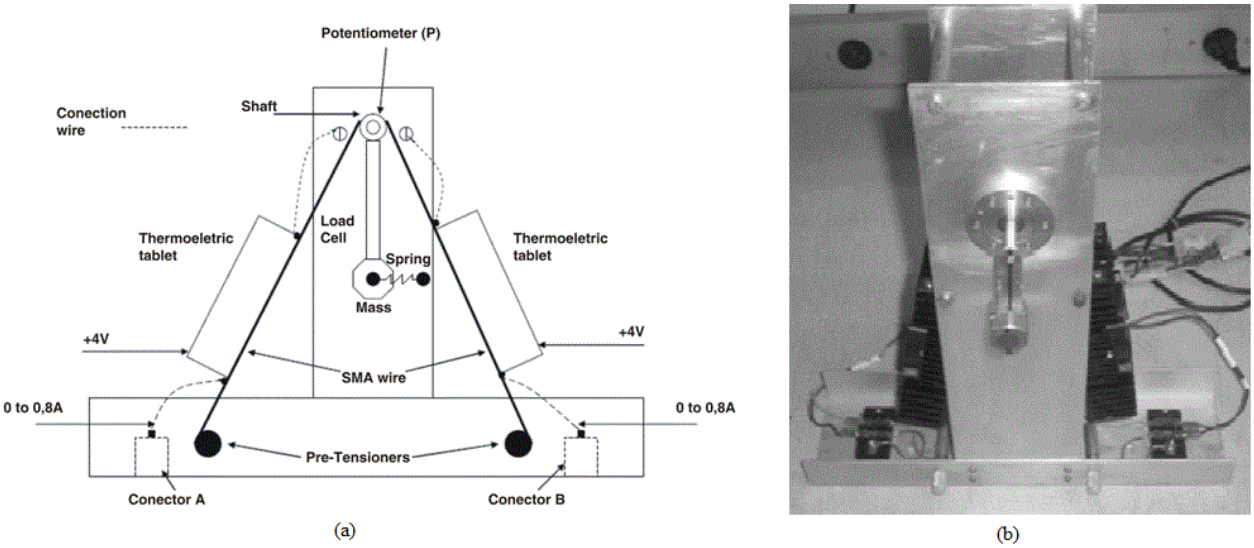

Figure 1- (a) Mechanical scheme of the antagonistic SMA actuator (b) Picture of the prototype, without a load cell (Source: Romano and Tannuri, 2009).

The wires are heated by current flowing through them. The current drive is a differential circuit that, for a given input divides the amount of current flowing through each wire. The difference between the currents guarantees the deflection or retraction of the wires and consequently the rotational positioning of the actuator.

An analog I/O USB board from Advantech is used to read the sensors input and provide the correct output to the drive. All the control and sensing operations are done through Matlab's Simulink and Advantech's API.

3. MATHEMATICAL MODEL

The mechanical system from Figure 1 can be described by eq. (1):

$$(J + ml^2)\ddot{\theta} + c\dot{\theta} + mgl\sin\theta = r(T_a - T_b) - T_l \tag{1}$$

Where J is the inertia of the rotation axis in kg.m², m is the weight of the pendulum in kg, l is the length of the pendulum in meters, θ is the angular position of the actuator in rad, c is the viscous damping in kg/s, g is the gravity acceleration in m/s², r is the radius of the rotating axis in meters, T_a and $T_b$are the tension in the "a" and "b" wires (in N) and T_l is the load torque.

The tension in the wires T_a and T_b changes as the elastic modulus of the nitinol changes, which is ruled by the martensitic concentration in the alloy. In Romano and Tannuri (2007) it was shown that we can describe this based in the actuator geometry and the mechanical properties of the nitinol wires. Eq. (2) describes the wires tension in f unction of the actuator's displacement and wire variables:

$$\begin{cases} T_a = K_0(1-\xi_a)(0{,}02l_{max} - r\theta) \\ T_b = K_0(1-\xi_b)(0{,}02l_{max} + r\theta) \end{cases} \tag{2}$$

With

$$K_0 = \frac{E_a A_{wire}}{l_0} \tag{3}$$

Ikuta et al (1991) proposed a sub layer phase transformation model that, according to its temperature derivative signal (if the wires are heating or cooling), follows the function described in eq. (4):

$$\xi_{a,b} = \begin{cases} \dfrac{\xi_M^{a,b}}{1+\exp\left[\dfrac{6{,}2}{\mathrm{A_f}-\mathrm{A_s}}\left(\mathrm{T_p^{a,b}}-\dfrac{\mathrm{A_s}+\mathrm{A_f}}{2}\right)\right]}, & \dot{T}>0 \\ \dfrac{1-\xi_A^{a,b}}{1+\exp\left[\dfrac{6{,}2}{\mathrm{M_s}-\mathrm{M_f}}\left(\mathrm{T_p^{a,b}}-\dfrac{\mathrm{M_s}+\mathrm{M_f}}{2}\right)\right]}+\xi_A^{a,b}, & \dot{T}<0 \end{cases} \quad (4)$$

Here, $\xi_{a,b}$ are the instantaneous martensite phase fractions referring to wires a or b, l_{max} is the maximum achievable length of the nitinol wire in meters, $E_a$is the elastic modulus of the austenitic phase in Pa, $A_{wire}$is the cross-sectional area of the wires in m^2, l_0 is the minimum achievable length of the nitinol wire in meters, $\xi_M^{a,b}$ are the highest martensite fraction during cooling, referring to wires a or b, $\xi_A^{a,b}$ are the initial values of martensite fraction during cooling, referring to wires a or b, $T_p^{a,b}$ are the temperatures in the wires a or b, A_f is the final temperature of austenite transformation, A_s is the initial temperature of austenite transformation, $M_f$is the final temperature of martensite transformation and M_s is the initial temperature of martensite transformation.

The temperatures T_p^a, T_p^b dynamics are given by heat transfer balance in eq. (5):

$$m_{wire}c_p\dot{T_p^{a,b}} = i_{a,b}^2R - hA\left(T_p^{a,b}-T_{amb}\right) - C\left(T_p^{a,b}-T_{tablet}\right) \quad (5)$$

Where $m_{wire}$is the wire mass per unity length in kg/m, c_p is the wires specific heat in J/kg°C, R is the wire's electric resistance in Ω/m, h is the natural convection coefficient in W/m²°C, A is the wire's external area per unity length in m²/m, $T_{amb}$is the ambient temperature in °C, C is the heat conduction coefficient in Wm/°C and $T_{tablet}$is the Peltier tablet surface temperature (°C).

4. PARAMETERS ESTIMATION

A difficult part of modeling may be the estimation of the actuator parameters, which may be very inaccurate. The parameters are the martensitic and austenitic phases end temperatures (A_s, A_f, M_s, M_f), the conduction heat transfer coefficient (C) and the mechanical system's inertia and viscous friction coefficient (J and c).

To find good approximation, experiments were performed applying controlled current in the wires and obtaining the system response in two phases. In the first one, to obtain the thermal coefficients, current was slowly applied to the system's maximum and minimum allowed input in ramp shape, and a Linear Quadratic Optimization Algorithm was used to minimize the error function, $(\theta-\theta_{est})^2$. After obtaining the thermal static parameters, a second experiment applying a sinusoidal input higher frequency (from 10 Hz down to 2 Hz) input was performed, in order to obtain the system's inertia and viscous friction. The differences between optimized model response and initial estimated parameters model response can be seen in

Figure 2 shows the model identification results. The parameter obtained were $A_s = 62.23$ °C, $A_f = 143$ °C, $M_s = 107.49$ °C, $M_f = 29.86$ °C, $C = 0.2$ W.m/°C, $J = 1.49 \times 10^{-8}$ kg.m² and $c = 0.0112$ kg.s.

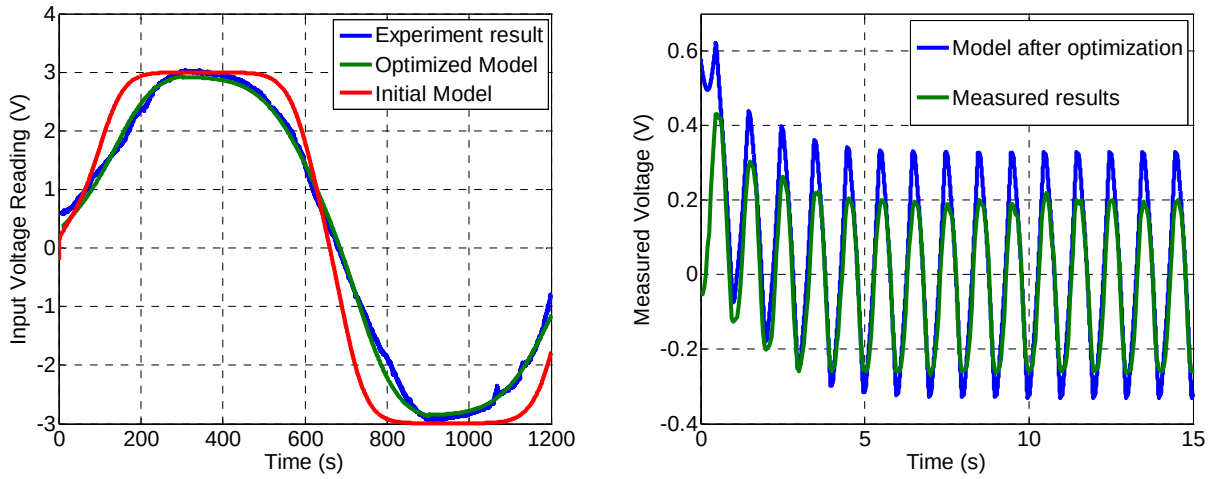

Figure 2 – (Right) Optimization results for open loop static response (cycle time = 1200s) and (left) results for open loop dynamic response (cycle time = 1 s).

5. CLOSED LOOP VALIDATION

To validate the optimization results and the numerical model, tests were performed applying a sliding mode control to the numerical model. The same control structure and parameters proposed by Romano and Tannuri (2009) were used in the simulations, and the experimental results presented in that work were compared to the results obtained by the numerical model

Figure 3 illustrates the results comparison for step response. It can be seen that the settling time obtained is practically the same (around 0.6 s for both).

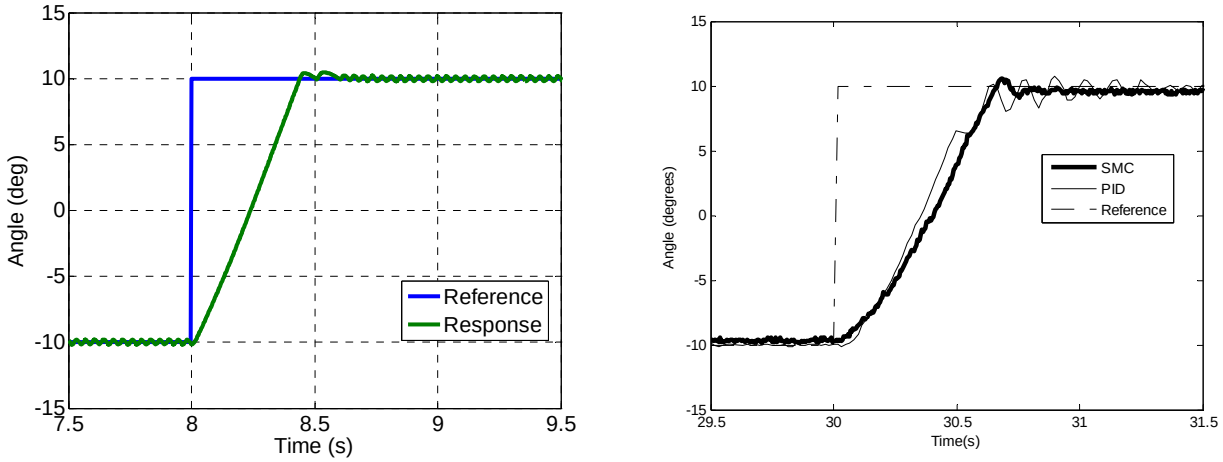

Figure 3 – Comparison of step response between (left) numerical model and (right) experimental results from Romano and Tannuri (2009).

Figure 4 shows the frequency response of the numerical model and the physical system. Cut off frequency was around 1.14 Hz for both, indicating the model is a very close approximation to the real system.

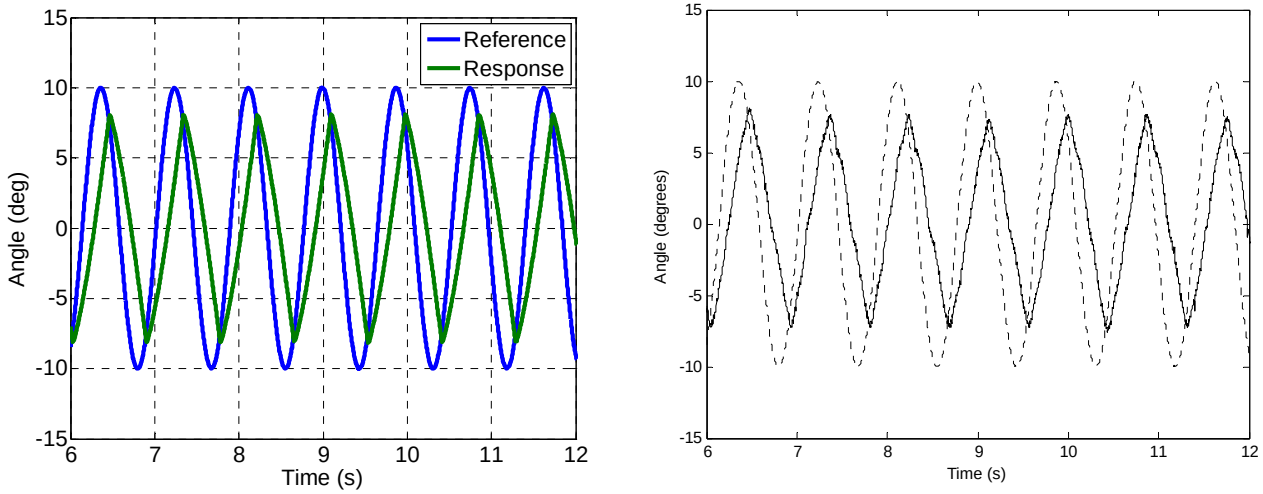

Figure 4 - Comparison of sine wave response between model (left) and (right) experimental results from Romano and Tannuri (2009).

6. CONTROL SYSTEM DESIGN

6.1. Angular Position control

The objective of the system is to control the rotational position of the actuator (θ) or to control the torque applied in the load (T_l). The controlled variable is the current applied to the wires.

To create a feedback control law (by feedback linearization or sliding modes) $u(\theta, \dot{\theta}, T_l, \xi_a, \xi_b)$, the modeled system must be organized in order to show the states as a function of the control input. First let's focus on position control, assuming no load is present ($T_l = 0$). In this case, external load is considered a perturbation.

Differentiating eq. (1):

$$(J + ml^2)\dddot{\theta} + c\ddot{\theta} + mgl\dot{\theta}\cos\theta = r(\dot{T}_a - \dot{T}_b) \tag{6}$$

After some algebra with the derivatives of eq. (2):

$$\begin{cases} \dot{T}_a = -\dot{\xi}_a K_0 \delta_a - (1 - \xi_a) K_0 r\dot{\theta} \\ \dot{T}_b = -\dot{\xi}_b K_0 \delta_b + (1 - \xi_b) K_0 r\dot{\theta} \end{cases} \tag{7}$$

Where

$$\begin{cases} \delta_a = 0{,}02 l_{max} - r\theta \\ \delta_b = 0{,}02 l_{max} + r\theta \end{cases} \tag{8}$$

$$\begin{cases} \ddot{\xi}_a = f_\xi(\xi_a) + b_\xi(\xi_a) u_a \\ \ddot{\xi}_b = f_\xi(\xi_b) + b_\xi(\xi_b) u_b \end{cases} \tag{9}$$

Here, $u_a = i_a^2$ and $u_b = i_b^2$. The functions f_ξ and b_ξ are given by equations (10) and (11):

$$f_\xi(\xi) = -\frac{\alpha}{\xi_0 m c_p}[\xi_0(\xi - k) - (\xi - k)^2]\left\{hAT_{amb} - CT_{tablet} - (hA + C)\left[\frac{1}{\alpha}\ln\left(\frac{\xi_0}{\xi - k} - 1\right) + \beta\right]\right\} \tag{10}$$

$$b_\xi(\xi) = -\frac{\alpha}{\xi_0 m c_p}[\xi_0(\xi - k) - (\xi - k)^2]R \tag{11}$$

The parameters in eq. (10) and (11) are different when heating or cooling occurs, following the next rule:

$$\begin{cases} \alpha = \dfrac{6{,}2}{A_f - A_s}; \beta = \dfrac{A_s + A_f}{2}; \xi_0 = \xi_M; k = 0 \quad if\ \dot{T}_p > 0 \\ \alpha = \dfrac{6{,}2}{M_s - M_f}; \beta = \dfrac{M_s + M_f}{2}; \xi_0 = 1 - \xi_A; k = \xi_a \quad if\ \dot{T}_p < 0 \end{cases}$$

Using eq. (7) and eq. (9) on the right end of eq. (6):

$$\dot{T}_a - \dot{T}_b = K_0\left[-\delta_a f_\xi(\xi_a) + \delta_b f_\xi(\xi_b) - \delta_a b_\xi(\xi_a) u_a + \delta_b b_\xi(\xi_b) u_b + r\dot{\theta}(\xi_a + \xi_b - 2)\right] \tag{12}$$

The differential electronic circuit that drives the wires imposes:

$$\begin{cases} i_a = 0{,}4 + \dfrac{u}{10} \\ i_b = 0{,}4 - \dfrac{u}{10} \end{cases} \tag{13}$$

Which gives:

$$\begin{cases} u_a = 0{,}16 + 0{,}08u + 0{,}01u^2 \\ u_b = 0{,}16 - 0{,}08u + 0{,}01u^2 \end{cases} \tag{14}$$

Finally, substituting eq. (14) in eq. (12) and inserting the result in eq. (6):

$$\begin{aligned} (J + ml^2)\dddot{\theta} = {} & -c\ddot{\theta} - mgl\dot{\theta}\cos\theta \\ & + rK_0\left\{-\delta_a f_\xi(\xi_a) + \delta_b f_\xi(\xi_b) + r\dot{\theta}(\xi_a + \xi_b - 2) + 0{,}16\left(\delta_b b_\xi(\xi_b) - \delta_a b_\xi(\xi_a)\right)\right\} \\ & - 0{,}08rK_0\left(\delta_a b_\xi(\xi_a) + \delta_b b_\xi(\xi_b)\right)u + 0{,}01rK_0\left(\delta_b b_\xi(\xi_b) - \delta_a b_\xi(\xi_a)\right)u^2 \end{aligned} \tag{15}$$

Equation (15) can be written as a function of the control input u:

$$\ddot{\theta} = f' + g'u + h'u^2 \tag{16}$$

The functions f', g' and h' are given by :

$$f' = \frac{1}{(J+ml^2)}\Big\{-c\ddot{\theta} - mgl\dot{\theta}\cos\theta + rK_0\left[-\delta_a f_\xi(\xi_a) + \delta_b f_\xi(\xi_b) + r\dot{\theta}(\xi_a + \xi_b - 2) + 0{,}16\left(\delta_b b_\xi(\xi_b) - \delta_a b_\xi(\xi_a)\right)\right]\Big\} \tag{17}$$

$$g' = \frac{-0{,}08rK_0}{(J+ml^2)}\left(\delta_a b_\xi(\xi_a) + \delta_b b_\xi(\xi_b)\right) \tag{18}$$

$$h' = \frac{-0{,}01rK_0}{(J+ml^2)}\left(\delta_a b_\xi(\xi_a) - \delta_b b_\xi(\xi_b)\right) \tag{19}$$

It can be seen from eq. (16) that the general form of the system if not affine with respect to the input. The following solution can be used both for feedback linearization and sliding mode control for this particular system.

First, we assume the following format:

$$\ddot{\theta} = f' + U \tag{20}$$

Where

$$U = g'u + h'u^2 \tag{21}$$

The root of eq. (21) can be real or imaginary, depending on the values that g', h' and U will assume. There are two situations:

$$\begin{cases}\Delta = g'^2 + 4h'U > 0 \Leftrightarrow u \in \mathbb{R} \\ \Delta = g'^2 + 4h'U < 0 \Leftrightarrow u \in \mathbb{C}\end{cases} \tag{22}$$

In the case $u \in \mathbb{R}$, the solution would be simply:

$$u = \frac{-g' \pm \sqrt{\Delta}}{2h'} \tag{23}$$

In the case $u \in \mathbb{C}$, there is not a real number that solves the problem. The best approximation for the solution of eq. (21) would be:

$$\min_u(h'u^2 + g'u - U) \tag{24}$$

In this case, control u that satisfies (24) would be:

$$u = -\frac{g'}{2h'} \tag{25}$$

6.1.1. Feedback Linearization Angular Position Control

Defining the tracking error for the control dynamic:

$$\tilde{\theta} = \theta - \theta_d \tag{26}$$

The desired feedback linearization control law to be input in eq. (21) is then:

$$U = -f' + \ddot{\theta}_d - K_1\tilde{\theta} - K_2\dot{\tilde{\theta}} - K_3\ddot{\tilde{\theta}} \tag{27}$$

Where θ_d is the desired trajectory of θ and K_1, K_2 and K_3 are linear control gains. The state variables ξ_a and ξ_b are assumed to be known through measured temperatures of the wires and the output derivatives of θ are obtained through low pass filter.

6.1.2. Sliding Modes Angular Position Control

For the sliding mode controller, sliding function s will be given by (Slotine and Li, 1991):

$$s = \ddot{\tilde{\theta}} + 2\lambda\dot{\tilde{\theta}} + \lambda^2\tilde{\theta} \tag{28}$$

Where λ is a positive constant related to the cut off frequency of the closed-loop system. The sliding function's derivative will be:

$$\dot{s} = \dddot{\theta} - \dddot{\theta}_d + 2\lambda\ddot{\tilde{\theta}} + \lambda^2\dot{\tilde{\theta}} = f' + U - \dddot{\theta}_d + 2\lambda\ddot{\tilde{\theta}} + \lambda^2\dot{\tilde{\theta}} \tag{29}$$

Finally the control law to achieve $\dot{s} = 0$ in the presence of unknown parameters will be

$$U = -\hat{f}' + \dddot{\theta}_d - 2\lambda\ddot{\tilde{\theta}} - \lambda^2\dot{\tilde{\theta}} - K_{SM}sat\left(\frac{s}{\phi}\right) \tag{30}$$

Here, $\hat{f}'$ is the best estimate of f', $K_{SM}$is a control gain related to the parameter and modeling errors, ϕ is the limit layer width, a parameter introduced to reduce chattering with an accuracy in control trade-off and $sat(s/\phi)$ is the saturation function:

$$sat\left(\frac{s}{\phi}\right) = \begin{cases} 1, & \frac{s}{\phi} > 1 \\ \frac{s}{\phi}, & -1 \le \frac{s}{\phi} \le 1 \\ -1, & \frac{s}{\phi} < 1 \end{cases} \tag{31}$$

6.2. Torque Control

Now, eq. (1) is differentiated, assuming the load is now different than zero and can be read through a load cell:

$$(J + ml^2)\dddot{\theta} + c\ddot{\theta} + mgl\dot{\theta}\cos\theta = r\left(\dot{T}_a - \dot{T}_b\right) - \dot{T}_l \tag{32}$$

Now, eq. (12) is substituted in eq. (32):

$$\begin{aligned} \dot{T}_l = rK_0\Big[&-\delta_a f_\xi(\xi_a) + \delta_b f_\xi(\xi_b) + r\dot{\theta}(\xi_a + \xi_b - 2) + 0{,}16\left(\delta_b b_\xi(\xi_b) - \delta_a b_\xi(\xi_a)\right) \\ &- 0{,}08u\left(\delta_a b_\xi(\xi_a) + \delta_b b_\xi(\xi_b)\right) + 0{,}01u^2\left(\delta_b b_\xi(\xi_b) - \delta_a b_\xi(\xi_a)\right)\Big] \\ &- (J + ml^2)\dddot{\theta} - c\ddot{\theta} - mgl\dot{\theta}\cos\theta \end{aligned} \tag{33}$$

Once again the following format is assumed:

$$\dot{T}_l = f'' + g''u + h''u^2 \tag{34}$$

Where

$$\begin{aligned} f'' = &-(J + ml^2)\dddot{\theta} - c\ddot{\theta} - mgl\dot{\theta}\cos\theta \\ &+ rK_0\left[-\delta_a f_\xi(\xi_a) + \delta_b f_\xi(\xi_b) + r\dot{\theta}(\xi_a + \xi_b - 2) + 0{,}16\left(\delta_b b_\xi(\xi_b) - \delta_a b_\xi(\xi_a)\right)\right] \end{aligned} \tag{35}$$

$$g'' = -0{,}08rK_0\left(\delta_a b_\xi(\xi_a) + \delta_b b_\xi(\xi_b)\right) \tag{36}$$

$$h'' = -0{,}01rK_0\left(\delta_a b_\xi(\xi_a) - \delta_b b_\xi(\xi_b)\right) \tag{37}$$

The same structure of eq. (20) is then proposed:

$$\dot{T}_l = f'' + U \tag{38}$$

6.2.1. Feedback Linearization Torque Control

Under the same conditions given by eq. (21) to (25), the desired feedback linearization control law for load torque control will be:

$$U = -f'' + \dot{T_{ld}} - K_1\widetilde{T_l} \tag{39}$$

With

$$\widetilde{T_l} = T_l - T_{ld} \tag{40}$$

Here, T_{ld} is the desired trajectory of T_l.

6.2.2. Sliding Modes Torque Control

The control surface s here will be:

$$s = \widetilde{T_l} = T_l - T_{ld} \tag{41}$$

And

$$\dot{s} = \dot{T_l} - \dot{T_{ld}} = f'' + U - \dot{T_{ld}} \tag{42}$$

The control U to achieve $\dot{s} = 0$ will be:

$$U = -\hat{f}'' + \dot{T_{ld}} - K_{SM}sat(s/\phi) \tag{43}$$

Again, $\hat{f}''$ represents the best approximation of f'' and K_{SM} is tuned to compensate modeling errors.

7. SIMULATION RESULTS AND DISCUSSION

7.1. Angular Position control

Figure 5 and fig. 6 illustrate angular position control results using feedback linearization and sliding modes control. The linear control gains from feedback linearization used were $K_1 = 100000$ $K_2 = 100$, $K3 = 1$. In sliding control, $K_{SM} = 16$, $\lambda = 500$ and $\phi = 2°$. Amplitude in both cases is of 10 degrees. A sampling rate of 500Hz was considered.

Cut off frequency is defined here as the frequency at which the system response amplitude is less than 0.707 times the input amplitude. It is clear that the results were slightly better using sliding modes control. Besides the higher cut off frequency, the curves format and phase are shown to be better shaped with sliding modes. The cost to this improvement is higher the control activity present in the better technique. Still, this control scheme is extremely robust and later experimental results are expected to have a very similar behavior.

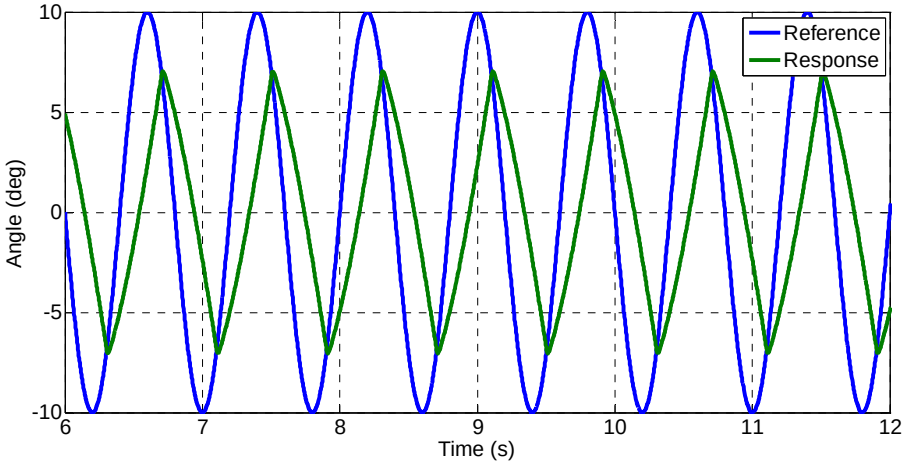

Figure 5 – Feedback Linearization results for angular position control. f = 1.25 Hz, $A/A_{reference} = 0.7$

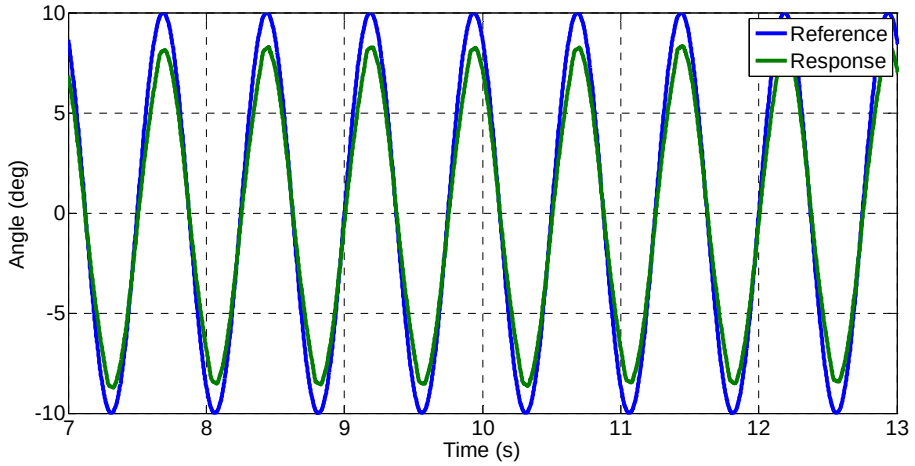

Figure 6 – Sliding Mode Control results for angular position control. f = 1.34 Hz, $A/A_{reference} = 0.8$

7.2. Torque Control

Figure 7 and fig. 8 show the results for torque control. An elastic load proportional to the angular position is added in the simulation. The spring constant considered is 0.02 N.m/rad. Linear control gain for feedback linearization is $K_1 = 1000$. Sliding control gain is $K_{SM} = 16$ and limit layer ϕ is 0.0005 N.m. Amplitude is 0.0035 N.m.

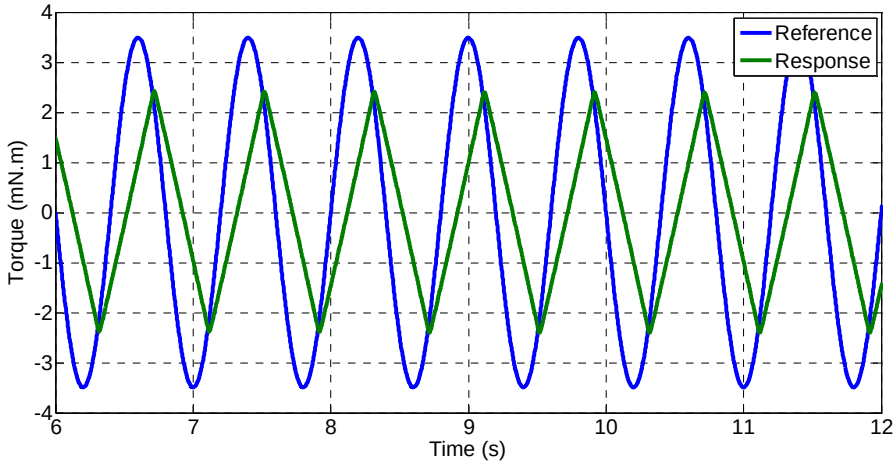

Figure 7 - Feedback Linearization results for torque control. f = 1.25 Hz, $A/A_{reference} = 0.7$

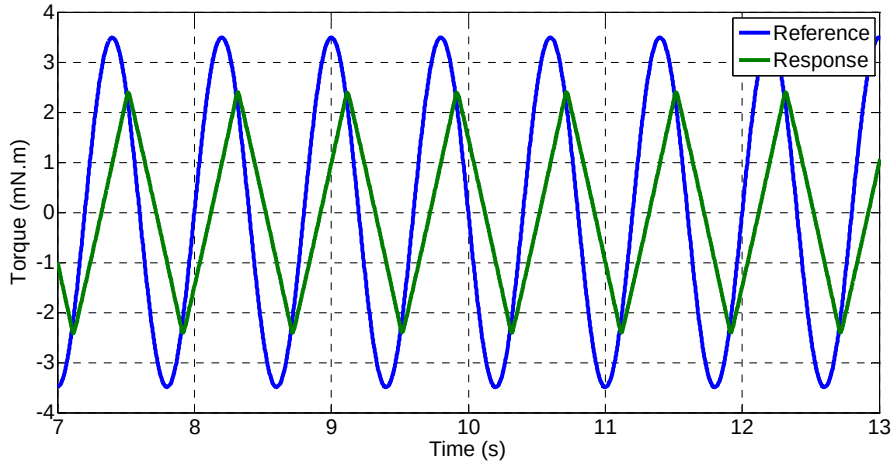

Figure 8 - Sliding Mode results for torque control. f = 1.25 Hz, $A/A_{reference} = 0.7$

Differently than the position control scheme, here the results were very close. Bandwidth achieved was o 1.25 Hz in both cases. Still, once again the results of the sliding mode scheme are expected to work better in the real system due to the robustness properties.

8. CONCLUSION

An antagonistic Shape Memory Alloy model was created and validated against several experiment results. Good curve fitting was obtained. Nonlinear control techniques based on the model were then developed and applied and simulated, obtaining enhanced results compared to control schemes that do not apply inverse dynamics. Force feedback control was proven to be stable, even though bandwidth was limited. Later experimental results are expected to behave in similar way.

9. ACKNOWLEDGEMENTS

The authors acknowledge Roberto Romano, from Institute for Technological Research - IPT, for the experimental support. The authors also acknowledge the National Council for Scientific and Technological Development (CNPq) for the research grant (301686/2007-6).

10. REFERENCES

Choi, S.B., Han, Y.M., Kim, J.H. and Cheong, C.C., 2001, "Force tracking control of a flexible gripper featuring shape memory actuators", Mechatronics 11, Elsevier Science Ltd., p. 677 - 690.

Elahinia, M.H., Seigler, T.M., Leo, D.J. and Ahmadian, M., 2004, "Nonlinear Stress-Based Control of a Rotary SMA-Actuated Manipulator", Journal of Intelligent Material Systems and Structures, Vol. 15, p. 495 - 508.

Grant, D. and Hayward, V., 2000, "Constrained Force Control of Shape Memory Alloy Actuators", Proceedings of the IEEE International Conference on Robotic and Automation, San Francisco, CA, p. 1314-1320.

Ikuta K., Tsukamoto M. and Hirose S., 1991, "Mathematical model and experimental verification of shape memory alloy for designing micro actuator", Proceedings of the IEEE on micro electromechanical systems, an investigation of microstructures, sensors, actuators, machines, and robots, p. 103-108.

Otubo, J., Mei, P.R. and Koshimizu, S., 1997, "Materials with Shape Memory Effect, main characteristics and possible applications", XIV Brazilian Congress of Mechanical Engineering, COBEM '97, Bauru, Brazil.

Romano, R. and Tannuri, E.A., 2007, "Modeling, control and experimental validation of a novel actuator based on shape memory alloys", XII International Symposium on Dynamic Problems of Mechanics, DINAME 2007, Ilhabela, Brazil.

Romano, R. and Tannuri, E.A., 2009, "Comparison between single-wire and antagonistic shape memory alloy actuators", XIII International Symposium on Dynamic Problems of Mechanics, DINAME 2009, Angra dos Reis, Brazil.

Slotine J.J.E. and Li W., "Applied nonlinear control", 1991, Prentice-Hall, Englewood Cliffs, USA, 461p.

Teh, Y.H. and Featherstone, R., 2007, "Accurate Force Control and Motion Disturbance Rejection for Shape Memory Alloy Actuators", Proceedings of the IEEE International Conference on Robotic and Automation, Roma, Italy, p. 10-14.

11. RESPONSIBILITY NOTICE

The authors are the only responsible for the printed material included in this paper.